J Mol Model (2012) 18:4955–4963
DOI 10.1007/s00894-012-1493-1

ORIGINAL PAPER

Ruthenium hydride-catalyzed regioselective addition of benzaldehyde to dienes leading to β,γ-unsaturated ketones: a DFT study

Qingxi Meng · Fen Wang · Ming Li

Received: 30 March 2012 / Accepted: 4 June 2012 / Published online: 22 June 2012

Abstract Density functional theory (DFT) was used to investigate the ruthenium hydride-catalyzed regioselective addition reactions of benzaldehyde to isoprene leading to the branched β,γ-unsaturated ketone. All intermediates and the transition states were optimized completely at the B3LYP/6-31 G(d,p) level (LANL2DZ(f) for Ru, LANL2DZ(d) for P and Cl). Calculated results indicated that three catalysts $RuHCl(CO)(PMe_3)_3$ (**1**), $RuH_2(CO)(PMe_3)_3$ (**2**), and $RuHCl(PMe_3)_3$ (**3**) exhibited different catalysis, and the first was the most excellent. The most favorable reaction pathway included the coordination of **1** to the less substituted olefin of isoprene, a hydrogen transfer reaction from ruthenium to the carbon atom C1, the complexation of benzaldehyde to ruthenium, the carbonyl addition, and the hydride elimination reaction. The carbonyl addition was the rate-determining step. The dominant product was the branched β,γ-unsaturated ketone. Furthermore, the presence of one toluene molecule lowered the activation free energy of the transition state of the carbonyl addition by hydrogen bonds between the protons of toluene and the chlorine, carbonyl oxygen of the ruthenium complex. On the whole, the solvent effect decreased the free energies of the species.

Keywords Benzaldehyde · β,γ-unsaturated ketones · DFT · Isoprene · Reaction mechanism · Ruthenium hydride-catalyzed addition

Introduction

Hydroacylation is an intriguing catalytic process because of its potential usefulness in the general synthesis of ketones from alkenes and aldehydes. Although the C-H bond activation by transition metal complexes often leads to decarbonylation, [1, 2] rhodium-catalyzed hydroacylation of alkenes or alkynes is one of the most useful C-H bond activation processes [3–10]. In 1998, employing Ru(cod)(cot)PPh_3 as a catalyst, Kondo and Mitsudo first reported ruthenium-catalyzed intermolecular hydroacylation of dienes with aldehydes [11].

Transition metal hydrides are involved in a variety of catalytic transformations and hydrometalation of such species to unsaturated bonds provides intermediates having metal-carbon or heteroatom bonds [12, 13]. Ruthenium hydride catalysts have played a large role in these important transformations [14–23]. Ryu and co-workers [22] reported the regioselective addition of aldehydes to unsaturated ketones catalyzed by $RuHCl(CO)(PPh_3)_3$ generating 1,3-diketones. Rencently, Ryu and co-workers [23] studied ruthenium hydride-catalyzed addition of aldehydes to dienes leading to β,γ-unsaturated ketones (Scheme 1), and suggested a likely mechanism (Scheme 2). They also showed that $RuHCl(CO)(PPh_3)_3$ gave the cross-addition product,

Electronic supplementary material The online version of this article (doi:10.1007/s00894-012-1493-1) contains supplementary material, which is available to authorized users.

Q. Meng (✉)
College of Chemistry and Material Science,
Shandong Agricultural University,
Taian, Shandong 271018, People's Republic of China
e-mail: qingxim@sdau.edu.cn

F. Wang
Department of Chemistry, Taishan University,
Taian, Shandong 271021, People's Republic of China

M. Li
College of Chemistry and Chemical Engineering,
Southwest University,
Chongqing 400715, People's Republic of China

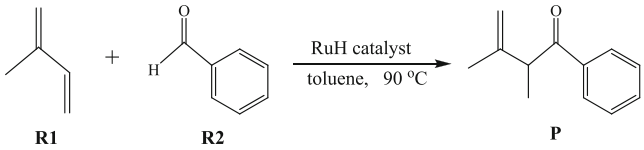

Scheme 1 Ruthenium hydride-catalyzed addition of benzaldehyde to dienes leading to β,γ-unsaturated ketones

2,3-dimethyl-1-phenyl-3-buten-1-one (**P**) in 95 % yield, and other catalysts, such as $RuH_2(CO)(PPh_3)_3$ and $RuHCl(PPh_3)_3$, gave a smaller amount of the product **P**.

In order to understand the reaction mechanism of ruthenium hydride-catalyzed addition of aldehydes to dienes leading to β,γ-unsaturated ketones in detail, the addition of aldehydes to dienes catalyzed by three Ru-H catalysts was studied in this work. Specifically, the present study would elucidate the following issues: (1) the energetics of the overall catalytic pathways in ruthenium hydride-catalyzed addition, (2) the structural features of intermediates and transition states involved, (3) why $RuHCl(CO)(PPh_3)_3$ was the better efficient catalyst than $RuH_2(CO)(PPh_3)_3$ and $RuHCl(PPh_3)_3$, and (4) the solvation effect in reaction mechanism. The most possible reaction pathway was outlined in Scheme 3.

Computational details

All calculations were carried out with the Gaussian 03 programs [24]. The geometries of all the species were fully optimized by using density functional theory (DFT) [25] of B3LYP method [26, 27]. The 6-31 G(d,p) basis set was used for the carbon, oxygen, and hydrogen atoms, and LANL2DZ basis set was used for ruthenium, phosphorus, and chlorine atoms by adding one set of *f*-polarization function to ruthenium (exponent: 1.235) [28] and one set of *d*-polarization function to phosphorus (exponent: 0.371) [29] and chlorine (exponent: 0.514) [29]. Frequency calculations at the same level were performed to confirm each stationary point to be either a minimum or a transition structure (**T**). The transition states were verified by intrinsic reaction coordinate (IRC) [30] calculations and by animating the negative eigenvector coordinates with a visualization program (Molekel 4.3) [31, 32]. The intermediates were characterized by all real frequencies. In addition, the bonding characteristics were analyzed by the natural bond orbital (NBO) theory [33–36]. NBO analysis was performed by utilizing NBO5.0 code [37] with the optimized structures. Furthermore, based on the gas phase optimized geometry for each species, the solvent effects of toluene were studied by performing a self-consistent reaction field (SCRF) [38, 39] of polarizable continuum model (PCM) [40] approach at the same computational level.

Molecular orbital compositions and the overlap populations were calculated with the AOMix program [41, 42]. The analysis of the MO compositions in term of occupied and unoccupied fragment molecular orbitals (OFOs and UFOs, respectively), the charge decomposition analysis (CDA), and the construction of orbital interaction diagrams were performed using AOMix-CDA [43]. In addition, the electron densities ρ at the bond critical points (BCPs) or the ring critical points (RCPs) for some species were calculated with the AIM 2000 program package [44, 45].

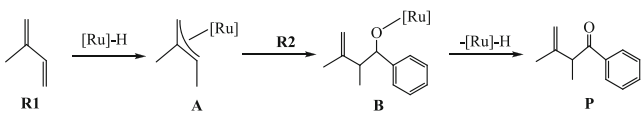

Scheme 2 Potential mechanism suggested by Ryu and co-workers [23]

Results and discussion

All optimized structures in the reaction mechanism were illustrated in Fig. S1~10. The relative free energies $\Delta G_{(sol)}$ including solvent energies, and the relative gas phase free energies ΔG, enthalpies ΔH, and ZPE corrected electronic energies ΔE were provided in Table S1~4. Unless otherwise noted, the discussed energies were relative free energies $\Delta G_{(sol)}$ in the following discussions.

The addition reactions catalyzed by the ruthenium-hydride catalyst $RuHCl(CO)(PMe_3)_3$

Figure 1 showed the potential energy hypersurface for the most favorable pathway leading to the branched β,γ-unsaturated ketone in the addition reactions catalyzed by $RuHCl(CO)(PMe_3)_3$ (**1**). Ruthenium hydride **1** coordinated to the less substituted olefin of isoprene (**R1**) to form the complex **1_M1a** and a free ligand PMe_3. Intermediate **1_M1a** underwent a hydrogen transfer reaction through the transition state **1_T1a** with a free energy of 20.6 kJ mol^{-1} leading to the complex **1_M2a** which isomerized the more stable complex **1_M3a**. Next, the complexation of benzaldehyde (**R2**) to **1_M3a** generated the complex **1_M4a** and a free ligand PMe_3. And then intermediate **1_M4a** went through a carbonyl addition via a six-centered transition state **1_T2a1** with a free energy of 45.0 kJ mol^{-1}, resulting in the ruthenium alkoxide complex **1_M5a1**. Finally, intermediate **1_M5a1** underwent a hydride elimination via a transition state **1_T3a1** with a free energy of 34.9 kJ mol^{-1} to deliver the complex **1_M6a1** giving the branched β,γ-unsaturated ketone. Hence, the formation of the ruthenium alkoxide complex **1_M5a1** (the carbonyl addition) was the rate-determining step for this pathway.

Scheme 3 The most possible reaction mechanism of ruthenium hydride-catalyzed addition of benzaldehyde to dienes leading to β,γ-unsaturated ketones

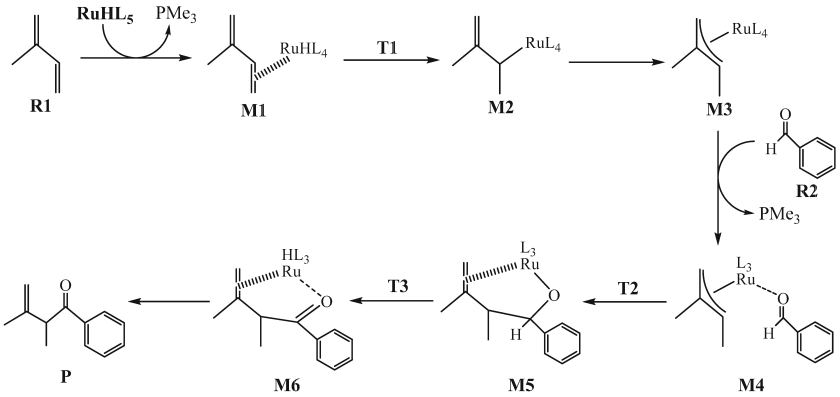

Intermediate **1_M1a** was a polarized complex with 2.201 and 2.304 Å of distances between Ru and two sp^2-hybridized carbon atoms C1 and C2, respectively (Fig. 2). The high stabilization energy of 288.4 kJ mol^{-1} for the $\sigma_{Ru\text{-}H1} \rightarrow (2p)_{C1}$, which was obtained from the second-order perturbation analysis of donor-acceptor interactions in the NBO basis and used to estimate the strengths of donor-acceptor interactions of the NBOs, revealed the strong interaction between $\sigma_{Ru\text{-}H1}$ and $(2p)_{C1}$ orbitals and the electron transfer tendency from $\sigma_{Ru\text{-}H1}$ to $(2p)_{C1}$. NBO analysis of **1_M1a** also showed there was a back-donation π bond between ruthenium and $\pi_{C1\text{-}C2}$ bond of isoprene: the occupied π bonding orbital ($\pi_{C1\text{-}C2}$) acted on the empty hybridized orbital of ruthenium leading to a σ coordinate bond; on the other hand, the occupied d orbital (d_{xy}, d_{xz}, d_{yz}) of ruthenium acted on the empty π* antibonding orbital ($\pi^*_{C1\text{-}C2}$) leading to a π back-donation bond. The formation of the back-donation π bond weakened and activated the C1-C2 bond, which resulted in the formation of C1-H1 bond. In hydrogen migration, the distance between Ru and H1, $d_{(Ru\text{-}H1)}$, increased, $d_{(C1\text{-}H1)}$ decreased, and Ru shifted to C2. It was clear that a significant interaction between C1 and H1 occurred, conversely the Ru-H1 bond was weakened considerably, as demonstrated by analyzing the changes of Wiberg bond orders P_{ij} and electron density ρ at the BCPs (e.g., Ru-H1 bond, P_{ij}, **1_M1a**: 0.665→**1_T1a**: 0.380→**1_M2a**: 0.014; ρ, **1_M1a**: 0.143→**1_T1a**: 0.112→**1_M2a**: 0.000 e·$Å^{-3}$). The Ru-C2 bond of **1_M2a** was a σ bond, while there was a back-donation π bond between ruthenium and a resonance-stabilized structure (Π_3^4) of C2, C3, C4 in **1_M3a** and **1_M4a**. The formation of the back-donation π bond made two complexes more stable. The complex **1_M3a** had been detected by H NMR in Ryu's experiment [23]. Transition state **1_T2a1** involved a Ru-O2-C6-C2-C3-C4 six-membered ring, and the electron density of the RCP was 0.015 e·$Å^{-3}$. As illustrated in Fig. 3, the HOMO-7 for **1_T2a1** was a mixture of 16.0 % HOFO-0 and 3.9 % HOFO-2 for benzaldehyde (fragment 1) and 18.6 % HOFO-3, 20.7 % HOFO-4, 7.6 % HOFO-5, 23.8 % HOFO-6 for ruthenium fragment (fragment 2). It was clear that the carbonyl addition between benzaldehyde and ruthenium fragment occurred dominantly between HOFO-0 of fragment 1 and HOFO-3, HOFO-4, HOFO-6 of fragment 2. The net charge donation, which included both charge donation and electronic polarization contributions, was 0.14 of electrons.

Furthermore, we have studied the other three reaction pathways leading to the other three linear or branched β,γ-unsaturated ketones: ruthenium hydride **1** coordinated to the more substituted olefin of isoprene to form the

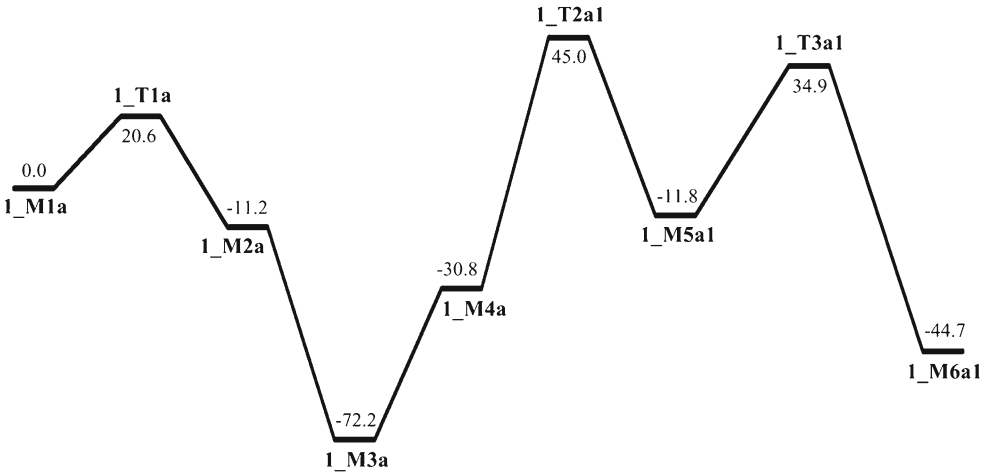

Fig. 1 Free energy profile for the most favorable pathway in Ru-catalyzed (RuHCl(CO)$(PMe_3)_3$ 1) addition reactions

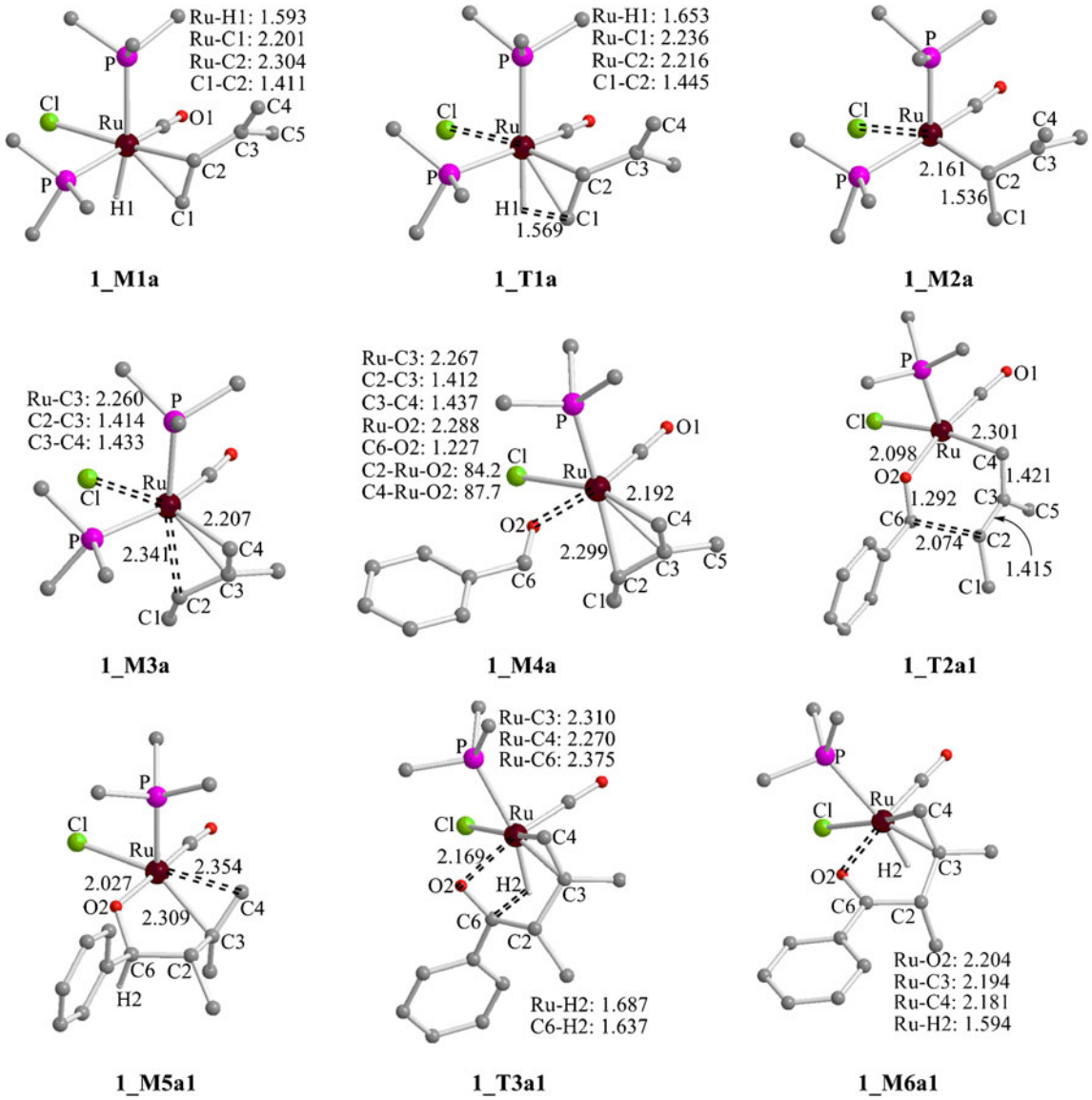

Fig. 2 Intermediates and transition states in the most favorable pathway in Ru-catalyzed ($RuHCl(CO)(PMe_3)_3$ **1**) addition reactions

complex **1_M1b**, and the carbonyl addition in the complexes **1_M4a** and **1_M4b** had two possible reaction pathways, respectively. In **1_M4a**, C6 attacking C2 was denoted "**a1**", while C6 attacking C4 was denoted "**a2**"; in **1_M4b**, C6 attacking C3 was denoted "**b1**", while C6 attacking C1 was denoted "**b2**". All the optimized structures were illustrated Figs. S1 and 2. In the three reaction pathways, the rate-determining step was also the formation of the ruthenium alkoxide complexes (the carbonyl addition) (Table S1).

The addition reactions catalyzed by the ruthenium-hydride catalyst $RuH_2(CO)(PMe_3)_3$

Figure 4 showed the potential energy hypersurface for the most favorable pathway leading to the branched β,γ-unsaturated ketone in the addition reactions catalyzed by $RuH_2(CO)(PMe_3)_3$ (**2**). Ruthenium hydride **2** coordinated to the less substituted olefin of isoprene to give the complex **2_M1a** and a free ligand PMe_3. Intermediate **2_M1a** underwent a hydrogen transfer reaction through the transition state **2_T1a** with a free energy of 41.1 kJ mol^{-1} resulting in the complex **2_M2a**. Next, the coordination of benzaldehyde to **2_M2a** generated the complex **2_M3a** and a free ligand PMe_3. And then intermediate **2_M3a** went through a carbonyl addition via a six-centered transition state **2_T2a1** with a free energy of 45.4 kJ mol^{-1}, leading to the ruthenium alkoxide complex **2_M4a1**. Finally, intermediate **1_M4a1** underwent a hydride elimination via a transition state **2_T3a1** with a free energy of 57.5 kJ mol^{-1} to deliver the complex **2_M5a1** forming the branched β,γ-unsaturated ketone. Clearly, the hydride elimination was the rate-determining step for this pathway.

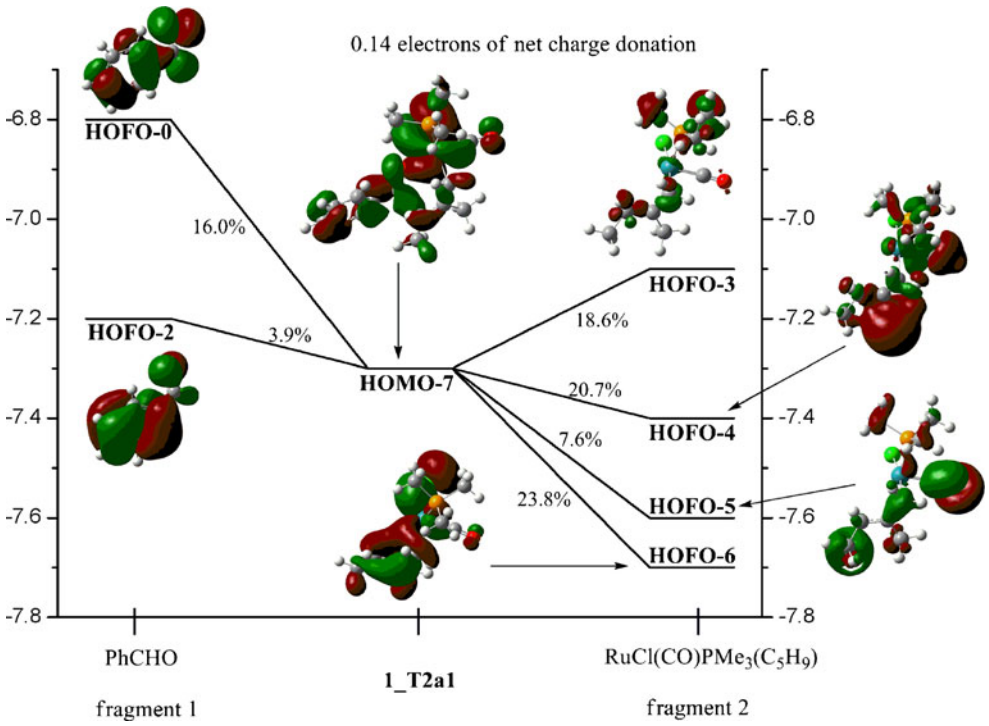

Fig. 3 Orbital interaction diagram for 1_T2a1 which is formed by PhCHO and RuCl(CO)$PMe_3(C_5H_9)$ (the AOMix-CDA calculation, based on B3LYP/6-31 G(d,p) results (LANL2DZ(f) for Ru, Cl and P). The net charge donation CT (1→2) - CT(2→1) is 0.14 electrons)

In intermediates **2_M2a** and **2_M3a**, Ru-C2, Ru-C3, and Ru-C4 bonds were about 2.23~2.37 Å (Fig. 5), and NBO analysis showed there was a back-donation π bond between ruthenium and a resonance-stabilized structure (Π_3^4) of C2, C3, C4. In this reaction pathway, we could not attain the structure with $\sigma_{Ru\text{-}C2}$ bond which was similar to **1_M2a**. Transition state **2_T2a1** involved a Ru-O2-C6-C2-C3-C4 six-membered ring, and the electron density of the RCP was 0.012 e·Å^{-3}. In **2_T3a1**, Ru-H3 was an σ bond, and C6 was sp^2-hybridized, C6 and O2 exhibited +0.955 and -0.626 of ATP charges. And there was a back-donation π bond between ruthenium and $\pi_{C3\text{-}C4}$ or $\pi_{C6\text{-}O2}$ bond.

In addition, we have studied the other two reaction pathways leading to the other two β,γ-unsaturated ketones: ruthenium hydride **2** coordinated to the more substituted olefin of isoprene to deliver the complex **2_M1b**, and the carbonyl addition in the complex **2_M3a** had two possible reaction pathways which could be coexistent, but the carbonyl addition in the complex **2_M3b** had only one reaction pathway because of different steric hindrance. (Fig. S3~4) In the two reaction pathways, the rate-determining step was also the hydride elimination.

The addition reactions catalyzed by the ruthenium-hydride catalyst $RuHCl(PMe_3)_3$

Figure 6 showed the potential energy hypersurface for the most favorable pathway leading to the branched β,γ-

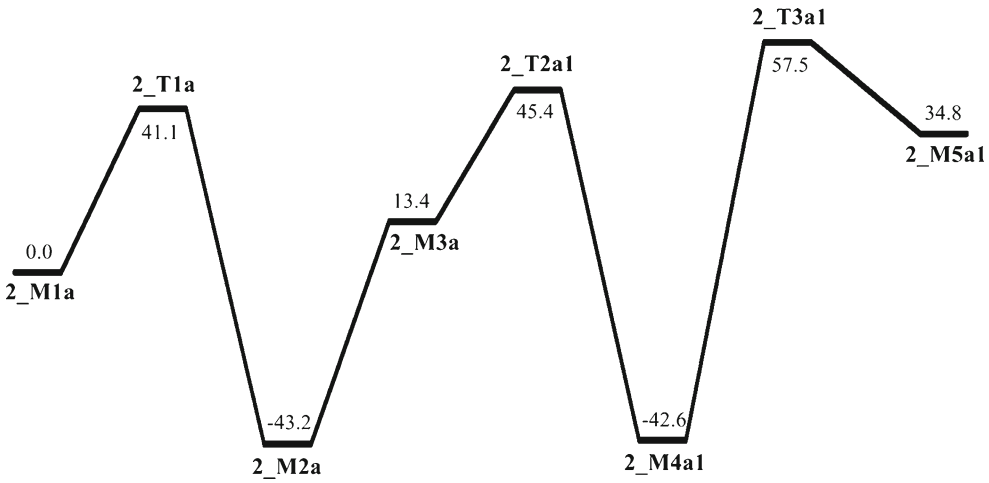

Fig. 4 Free energy profile for the most favorable pathway in Ru-catalyzed ($RuH_2(CO)(PMe_3)_3$ 2) addition reactions

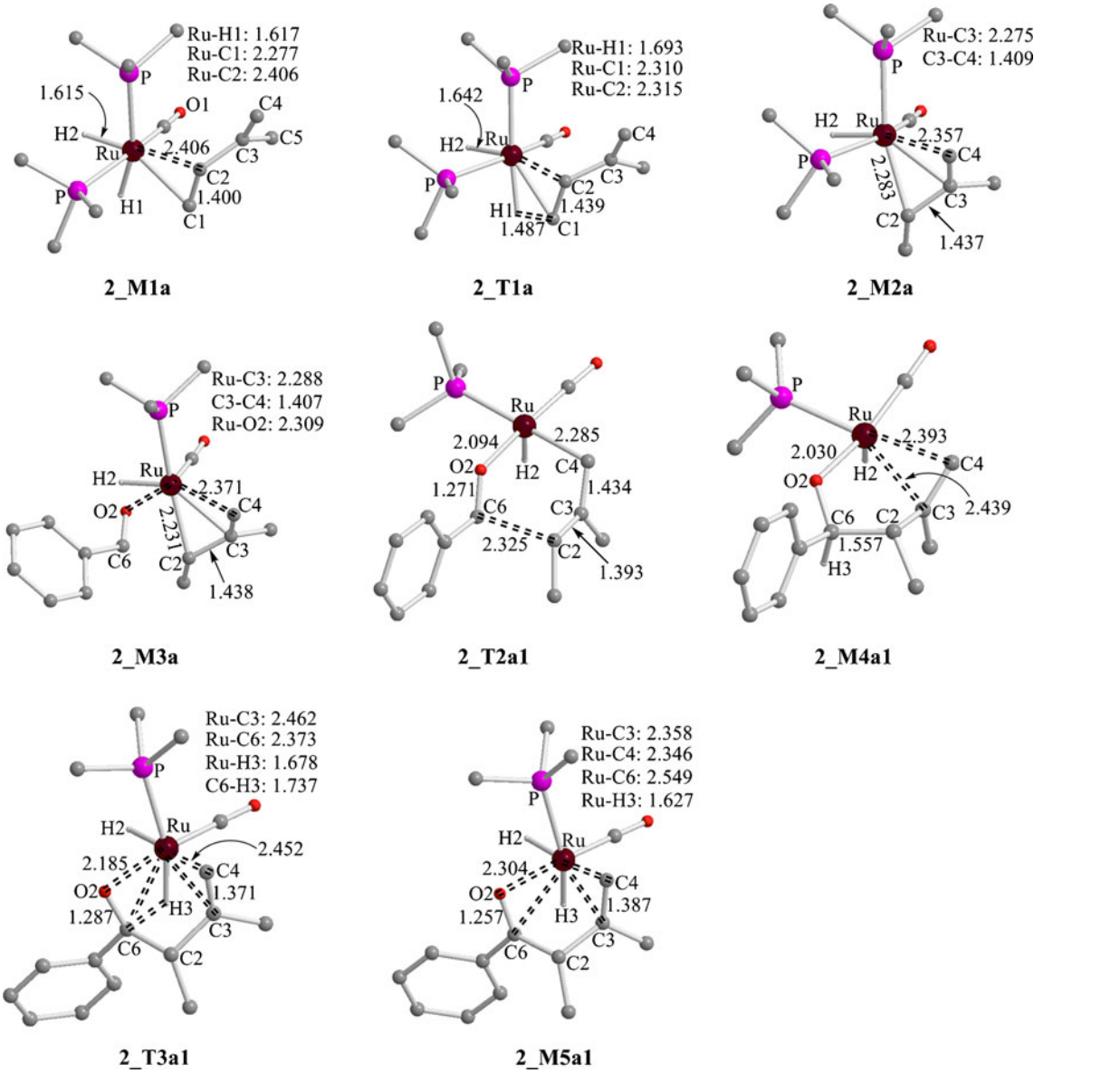

Fig. 5 Intermediates and transition states in the most favorable pathway in Ru-catalyzed ($RuH_2(CO)(PMe_3)_3$ 2) addition reactions

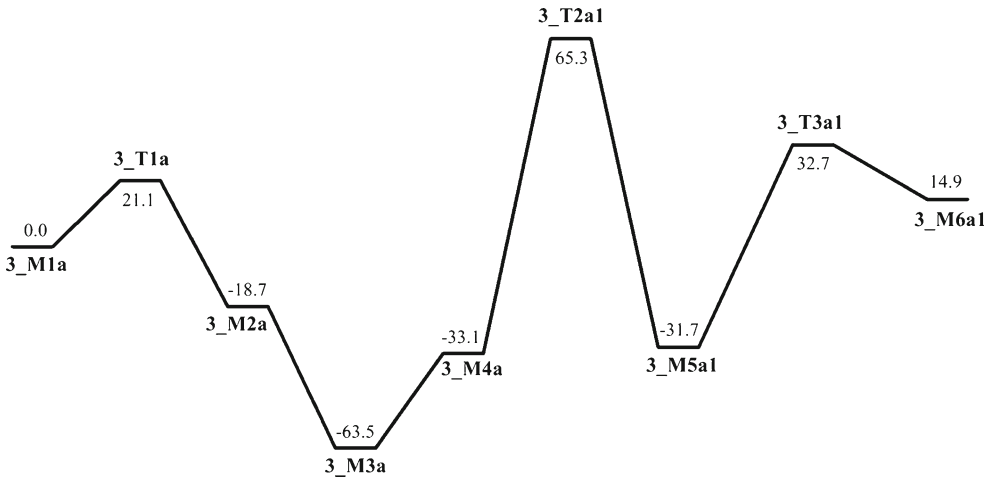

Fig. 6 Free energy profile for the most favorable pathway in Ru-catalyzed (RuHCl $(PMe_3)_3$ 3) addition reactions

unsaturated ketone in the addition reactions catalyzed by $RuHCl(PMe_3)_3$ (**3**). Ruthenium hydride **3** coordinated directly to the less substituted olefin of isoprene to form the six-coordinate complex **3_M1a**. The intermediates and transition states in the sequent reaction were similar to those discussed in $RuHCl(CO)(PMe_3)_3$-catalyzed addition (Fig. 7). The free energies of **3_T1a**, **3_T2a1**, **3_T3a1** were, respectively, 21.1, 65.3, 32.7 kJ mol^{-1}. Evidently, the formation of the ruthenium alkoxide complex **3_M5a1** (the carbonyl addition) was the rate-determining step for this pathway.

In addition, we have studied the other two reaction pathways leading to the other two β,γ-unsaturated ketones: ruthenium hydride **3** coordinated to the more substituted olefin of isoprene to form the complex **3_M1b**, and the carbonyl addition in the complex **3_M3a** had two possible reaction pathways, but the carbonyl addition in the complex **3_M3b** had only one reaction pathway because of different steric hindrance (Figs. S5 and 6). In the two reaction pathways, the rate-determining step was the formation of the ruthenium alkoxide complexes (the carbonyl addition).

Ruthenium hydride **3** was five-coordinate complex, so it could coordinate to the less substituted olefin of isoprene to generate the five-coordinate ruthenium complex **3_M1c** and a free ligand PMe_3 (Fig. S7). The free energies of **3_T1c**, **3_T2c**, **3_T3c** were, respectively, 89.0,

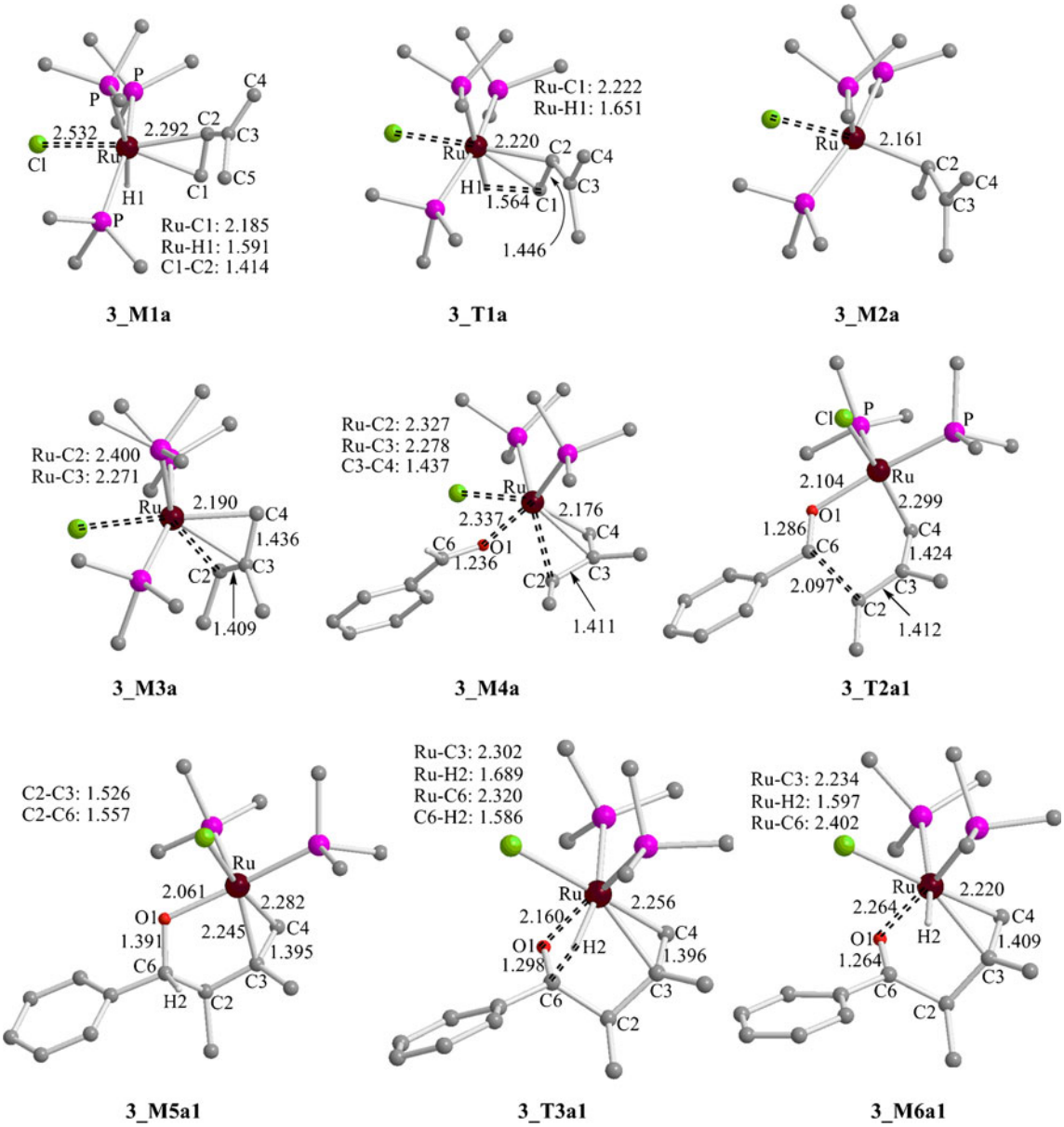

Fig. 7 Intermediates and transition states in more favorable pathway in Ru-catalyzed ($RuHCl(PMe_3)_3$ 3) addition reactions

247.7, 153.6 kJ mol^{-1}. In this pathway, the rate-determining step was also the carbonyl addition. Obviously, the free energy of **3_T2c** was higher than **3_T2a1** by 182.4 kJ mol^{-1}, so this pathway was prohibited.

Overview of the reaction mechanism

As discussed above, we have studied the addition reactions catalyzed by three catalysts RuHCl(CO)(PMe_3)$_3$, RuH_2(CO)(PMe_3)$_3$, and RuHCl(PMe_3)$_3$. In RuHCl(CO)(PMe_3)$_3$-catalyzed process, the carbonyl addition was the rate-determining step ($\Delta G(sol)_{\mathbf{1\_T2a1}}$=45.0 kJ mol^{-1}, Fig. 1). In RuH_2(CO)(PMe_3)$_3$ -catalyzed process, the hydride elimination was the rate-determining step ($\Delta G(sol)_{\mathbf{2\_T3a1}}$=57.5 kJ mol^{-1}, Fig. 4). In RuHCl(PMe_3)$_3$-catalyzed process, the carbonyl addition was the rate-determining step ($\Delta G(sol)_{\mathbf{3\_T2a1}}$= 65.3 kJ mol^{-1}, Fig. 6). Clearly, the free energy of **1_T2a1** was lower than those of **2_T3a1** and **3_T2a1**, and then RuHCl(CO)(PMe_3)$_3$ was the most excellent catalyst, which agreed with these experiments [23]. Therefore, the reaction pathway illustrated in Fig. 1 was the most favorable in the overall reaction channels of the addition reactions catalyzed by ruthenium hydride.

The free energy barriers of all transition states has been summarized in Table S5. Several results due to the free energy barriers were summarized as follows: (1) the rate-determining steps of three catalysts-catalyzed processes remained unchangeable. (2) Because the free energy barrier of **1_T2a1** was lower than those of **2_T3a1** and **3_T2a1** ($\Delta G^{\neq}(sol)_{\mathbf{1\_T2a1}}$=75.8, $\Delta G^{\neq}(sol)_{\mathbf{2\_T3a1}}$=100.1, $\Delta G^{\neq}(sol)_{\mathbf{3\_T2a1}}$=98.4 kJ mol^{-1}), the reaction pathway catalyzed by RuHCl(CO)(PMe_3)$_3$ illustrated in Fig. 1 was the most favorable in the addition reactions. (3) Three catalysts RuHCl(CO)(PMe_3)$_3$, RuH_2(CO)(PMe_3)$_3$, and RuHCl(PMe_3)$_3$ exhibited different catalysis, and the first was remarkably the most excellent, which agrees with these experiments [23].

As demonstrated above, the catalyst RuHCl(CO)(PMe_3)$_3$ exhibited the most excellent catalysis. The most favorable reaction pathway began with the coordination of **1** to the less substituted olefin of isoprene to form **1_M1a**. Then, a hydrogen transfer reaction from ruthenium to the carbon atom C1 to give the complex **1_M2a** which isomerized the more stable complex **1_M3a**. Next, the complexation of benzaldehyde to ruthenium to generate the complex **1_M4a**. Further, a carbonyl addition to form the ruthenium alkoxide complex **1_M5a1**. Finally, a hydride elimination to deliver the complex **1_M6a1** giving the branched β,γ-unsaturated ketone.

The effect of the explicit solvent

Ryu et al. reported the addition reaction to proceed smoothly in toluene and 95 % high yield. We were interested in the effect of toluene for the reaction. The intermediate and transition structures on the most favorable pathway were located in the presence of one toluene molecule. The optimized structures of all intermediates and transition states were shown in Fig. S10. As illustrated in Fig. S9, the activation free energy of **1_T2a1(t)** was 4.9 kJ mol^{-1} lower than that of **1_T2a1** in the absence of solvent in Fig. 1. The toluene protons interacted with the chlorine and carbonyl oxygen of the ruthenium complex (The distances of hydrogen bonds were shown in Fig. S10.), withdrew electrons from the ruthenium complex, and increased the electrophilicity of the allyl part, which would result in a carbonyl addition.

In addition, to evaluate the solvent effect for toluene (ε=2.379), single-point computations have been performed at the B3LYP/6-31 G(d,p) level (LANL2DZ(f) for Ru, LANL2DZ(d) for P and Cl) using the PCM model with default parameters, except for the temperature (363.15 K was used). In general, the solvation effect was remarkable, and it decreased the free energies of the species (Tables S1-4).

Conclusions

The reaction mechanisms of ruthenium hydride-catalyzed regioselective addition reactions of benzaldehyde to isoprene leading to the branched β,γ-unsaturated ketone were explored computationally using DFT (B3LYP/6-31 G(d,p) level, LANL2DZ(f) for Ru, LANL2DZ(d) for P and Cl). Calculated results indicated that three catalysts RuHCl(CO)(PMe_3)$_3$ (**1**), RuH_2(CO)(PMe_3)$_3$ (**2**), and RuHCl(PMe_3)$_3$ (**3**) exhibited different catalysis, and the first was the most excellent. The most favorable reaction pathway began with the coordination of **1** to the less substituted olefin of isoprene to form **1_M1a**. Then, a hydrogen transfer reaction from ruthenium to the carbon atom C1 to give the complex **1_M2a** which isomerized the more stable complex **1_M3a**. Next, the complexation of benzaldehyde to ruthenium to generate the complex **1_M4a**. Further, a carbonyl addition to form the ruthenium alkoxide complex **1_M5a1**. Finally, a hydride elimination to deliver the complex **1_M6a1** giving the branched β,γ-unsaturated ketone. The carbonyl addition was the rate-determining step. The dominant product was the branched β,γ-unsaturated ketone **P1**.

Furthermore, the presence of one toluene molecule lowered the activation free energy of the transition state of the carbonyl addition by hydrogen bonds. In general, the solvation effect was remarkable, and it decreased the free energies of the species.

Acknowledgments This work was supported by Natural Science Foundation of Shandong Province, P. R.

References

1. Colquhoun HM, Thompson DJ, Twigg MV (1991) Carbonylation: direct synthesis of carbonyl compounds. Plenum, New York, p 205
2. Bates RW (1995) In: Abel EW, Stone FGA, Wilkinson G (eds) Comprehensive organometallic chensitry II, vol 12. Pergamon, Oxford, p 373
3. Tanaka K, Fu GC (2001) J Am Chem Soc 123:11492–11493
4. Willis MC, Sapmaz S (2001) Chem Commun 2001:2558–2559
5. Jun CH, Moon CW, Lee DY (2002) Chem Eur J 8:2422–2428
6. Tanaka K, Fu GC (2003) J Am Chem Soc 125:8078–8079
7. Takeishi K, Sugishima K, Sasaki K, Tanaka K (2004) Chem Eur J 10:5681–5688
8. Jun CH, Jo EA, Park JW (2007) Eur J Org Chem 2007:1869–1881
9. Roy AH, Lenges CP, Brookhart M (2007) J Am Chem Soc 129:2082–2093
10. Moxham GL, Randell-Sly H, Brayshaw SK, Weller AS, Willis MC (2008) Chem Eur J 14:8383–8397
11. Kondo T, Hiraishi N, Morisaki Y, Wada K, Watanabe Y, Mitsudo T (1998) Organometallics 17:2131–2134
12. Beller M, Bolm C (eds) (1998) Transition metals for organic synthesis, vol 1 and 2. Wiley, Weinheim
13. Cornils B, Herrmann AW (eds) (1996) Applied homogeneous catalysis with organometallic compounds, vol 1 and 2. Wiley, Weinheim
14. Clapham SE, Hadzovic A, Morris RH (2004) Coord Chem Rev 248:2201–2237
15. Schmidt B (2004) Eur J Org Chem 2004:1865–1880
16. Arisawa M, Terada Y, Takahashi K, Nakagawa M, Nishida A (2006) J Org Chem 71:4255–4261
17. Burling S, Paine BM, Nama D, Brown VS, Mahon MF, Prior TJ, Pregosin PS, Whittlesey MK, Williams JMJ (2007) J Am Chem Soc 129:1987–1995
18. Casey CP, Clark TB, Guzei IA (2007) J Am Chem Soc 129:11821–11827
19. Shibahara F, Bower JF, Krische MJ (2008) J Am Chem Soc 130:6338–6339
20. Shibahara F, Bower JF, Krische MJ (2008) J Am Chem Soc 130:14120–14122
21. Denichoux A, Fukuyama T, Doi T, Horiguchi J, Ryu I (2010) Org Lett 12:1–3
22. Fukuyama T, Doi T, Minamino S, Omura S, Ryu I (2007) Angew Chem Int Ed 46:5559–5561
23. Omura S, Fukuyama T, Horiguchi J, Murakami Y, Ryu I (2008) J Am Chem Soc 130:14094–14095
24. Klene M, Li X, Knox JE, Hratchian HP, Cross JB, Adamo C, Jaramillo J, Gomperts R, Stratmann RE, Yazyev O, Austin AJ, Cammi R, Pomelli C, Ochterski JW, Ayala PW, Morokuma K, Voth GA, Salvador P, Dannenberg JJ, Zakrzewski VG, Dapprich S, Daniels AD, Strain MC, Farkas O, Malick DK, Rabuck AD, Raghavachari K, Foresman JB, Ortiz JV, Cui Q, Baboul AG, Clifford S, Cioslowski J, Stefanov BB, Liu G, Liashenko A, Piskorz P, Komaromi I, Martin RL, Fox DJ, Keith T, Al-Laham MA, Peng CY, Nanayakkara A, Challacombe M, Gill PMW, Johnson B, Chen W, Wong MW, Gonzalez C, Pople JA (2004) Gaussian 03, Revision B.05. Gaussian Inc, Pittsburgh
25. Parr RG, Yang W (1989) Density-functional theory of atoms and molecules. Oxford University Press, New York
26. Becke AD (1993) J Chem Phys 98:5648–5652
27. Lee C, Yang W, Parr RG (1988) Phys Rev B 37:785–789
28. Ehlers AW, Böhme M, Dapprich S, Gobbi A, Höllwarth A, Jonas V, Köhler KF, Stegmann R, Veldkamp A, Frenking G (1993) Chem Phys Lett 208:111–114
29. Check CE, Faust TO, Bailey JM, Wright BJ, Gilbert TM, Sunderlin LS (2001) J Phys Chem A 105:8111–8116
30. Gonzalez C, Schlegel HB (1990) J Phys Chem 94:5523–5527
31. Flükiger P, Lüthi HP, Portmann S, Weber J (2000-2002) MOLEKEL 4.3 Swiss Center for Scientific Computing, Manno. Switzerland
32. Portmann S, Lüthi HP (2000) Chimia 54:766–770
33. Carpenter JE, Weinhold F (1988) J Mol Struct Theochem 169:41–50
34. Foster JP, Weinhold F (1980) J Am Chem Soc 102:7211–7218
35. Reed AE, Weinstock RB, Weinhold F (1985) J Chem Phys 83:735–746
36. Reed AE, Curtiss LA, Weinhold F (1988) Chem Rev 88:899–926
37. Glendening ED, Badenhoop JK, Reed AE, Carpenter JE, Bohmann JA, Morales CM, Weinhold F (2001) NBO 5.0, Theoretical Chemistry Institute, University of Wisconsin, Madison, WI
38. Marten B, Kim K, Cortis C, Friesner RA, Murphy RB, Ringnalda MN, Sitkoff D, Honig B (1996) J Phys Chem 100:11775–11788
39. Friesner RA, Murphy RB, Beachy MD, Ringnalda MN, Pollard WT, Dunietz BD, Cao YX (1999) J Phys Chem A 103:1913–1928
40. Miertus S, Tomasi J (1982) Chem Phys 65:239–245
41. Gorelsky SI, Lever ABP (2001) J Organomet Chem 635:187–196
42. Gorelsky SI (1997) AOMix: Program for molecular orbital analysis. York University, Toronto, http://www.sf-chem.net/
43. Gorelsky SI, Ghosh S, Solomon EI (2006) J Am Chem Soc 128:278–290
44. Bader RFW (1990) Atoms in molecules, a quantum Theory; International series of monographs in chemistry, vol 22. Oxford University Press, Oxford
45. Biegler-König F, Schönbohm J, Derdau R, Bayles D, Bader RFW (2002) AIM 2000. Version 2.0, McMaster University, Hamilton, Canada